Reprinted from the Journal of the American Ceramic Society, Vol. 68, No. 11, November 1985.
Copyright 1985 by The American Ceramic Society

Strength and Fatigue Properties of Optical Glass Fibers Containing Microindentation Flaws

TIMOTHY P. DABBS*

Department of Applied Physics, School of Physics, University of New South Wales, N.S.W. 2033, Australia

BRIAN R. LAWN*

Center for Materials Science, National Bureau of Standards, Gaithersburg, Maryland 20899

The inert strength and dynamic fatigue properties of fused-silica optical fibers are studied using *subthreshold* indentation flaws, i.e., flaws without radial cracks. These subthreshold properties differ from those obtained in comparative tests on silica rods containing *postthreshold* indentation flaws in three major respects: (1) the inert strengths are significantly higher than predicted by extrapolation of the postthreshold data; (2) the slopes of the dynamic fatigue plots are likewise greater, indicating a greater susceptibility of the subthreshold flaws to chemical kinetic effects; and (3) the scatter in strengths is wider. These trends reflect the change in mechanical response reported for optical fibers with "natural" flaw populations in going from ordinary to ultra-high-strength regions. Direct observations of the indentation sites up to the point of failure indicate that the property differences can be interpreted in terms of a transition from propagation-controlled to initiation-controlled fracture instabilities at reduced contact loads. The subthreshold instability condition is modeled qualitatively as a two-step, deformation-fracture process, with strong emphasis on the importance of residual stress fields in parametric evaluations. The relevance of the results to the practical issue of fiber reliability, most notably in connection with the potential dangers of using macroscopic crack velocity data to predict long-lifetime characteristics, is addressed.

I. Introduction

THE PRODUCTION of optical-quality glass fibers with ultrahigh strengths (>5 GPa) over long lengths (>5 km) is now technically feasible.[1-3] The key to sustaining such strength levels is the avoidance of any stress-concentrating sources (e.g., dust particles) at all times after initial drawing of the pristine fiber, so that the surfaces might remain free of microscopic "flaws." Once created, flaws can evolve with time, particularly in the presence of water-containing environments, thereby causing the strength of the fibers to degrade progressively, i.e., to "fatigue."[4-11] There are some precautions that can be taken to minimize strength degradation, for example by appropriate coating and packaging of the pristine fibers. However, the optimal use of any such fiber product rests, as for all brittle materials, with a proper understanding of the underlying micromechanical processes which can lead to failure.

Until now the common approach to a design philosophy has been to assert that the strength-degrading flaws are "microcracks," scaled-down versions of the macroscopic crack configurations generally used in fracture mechanics studies on bulk glasses.[12,13] Then the well-established "laws" of crack growth obtained from the latter studies may be assumed to hold equally well in the microscopic region; the problem is reduced to purely geometrical terms, whereby the strength properties are determined by some characteristic "flaw size." Unfortunately, it is not generally possible to specify this flaw size a priori for any given fiber; experimental techniques for locating and quantifying the severity of potential failure sources are not yet available. Consequently, the design engineer has had to proceed along a statistical front, assuming that the critical flaw is a member of some well-defined (e.g., Weibull) population, the functional parameters of which may be evaluated by laboratory testing of a sufficiently large sample of specimens.[7,14]

Moreover, there is cumulating evidence that fracture parameters evaluated in strength tests on optical-quality fibers differ significantly from those evaluated in comparable tests on bulk glass.[15] An important case in point is the (inverse) "fatigue susceptibility" parameter, n, determined from the slopes of strength vs stressing rate ("dynamic fatigue") plots. Values of this parameter tend to be much lower than those obtained from crack velocity data on bulk glass, by as much as one half at the higher strength levels. Thus for fused silica in water environments, strength measurements on pristine fibers give $n \approx 20$,[2,7,8-10] whereas direct measurements of the crack velocity exponent give $n \approx 36$ to 41.[16,17] There is the suggestion that the simplistic macroscopic crack growth flaws may no longer apply in the region of ultrasmall flaws, thereby casting a shadow on the entire fracture mechanics theory of strength in this region.

One experimental technique which overcomes the objection of working with an ill-defined flaw system is that of indentation.[18-30] By deliberately contacting the surface of a prospective strength test specimen with a Vickers hardness indenter one introduces a "controlled flaw" whose geometry and location can be predetermined accurately. Direct observation of the evolution of such artificial flaws, from initial formation during the indentation cycle to growth to failure during the subsequent strength test,[18-20,28,29] has provided new insights into the general micromechanics of flaw response. Chief among these is the crucial role of residual driving forces (associated in the present case with the irreversible component of the contact field[20]) throughout the entire evolution of the radial crack system.[18,19,28,29] This role is manifest in time-dependent strength characteristics as an increase in the fatigue susceptibility: whereas the n value for glass surfaces containing *residual-stress-free* indentations (e.g., surfaces subjected to a postcontact anneal) with well-developed radial cracks corresponds to that determined from independent velocity measurements, the apparent value for *as-indented* surfaces is about one quarter lower.[21,22] We may recall from the previous paragraph that the apparent n value for high-strength optical fibers is also lower, although the discrepancy factor there was about one half. Could it be that the "natural" strength-degrading flaws in the fibers, insofar as they can be considered to retain the identity of true microcracks, are subject to essentially similar, if stronger, residual driving forces?

It is this line of thinking which has prompted recent attention to indentation flaw response at low loads. Herein lies one of the unique advantages of the indentation methodology: one has the facility to control the *size* of the flaw, via the contact load, allowing for systematic study of fracture laws on going from macroscopic to microscopic dimensions. It is well-known that there is an abrupt threshold in the load, below which the indentations no longer generate radial cracks.[31] For silicate glasses this threshold occurs at ≈ 10 μm in flaw size, although the critical condition is highly sensitive to test environment, especially water.[28-30] Questions arise as to whether these subthreshold flaws retain the capacity to degrade the strength and, if so, whether the residual stress

Received February 25, 1985; revised copy received June 10, 1985; approved August 2, 1985.
Supported in part by the U.S. Office of Naval Research, Metallurgy and Ceramics Program.
*Member, the American Ceramic Society.

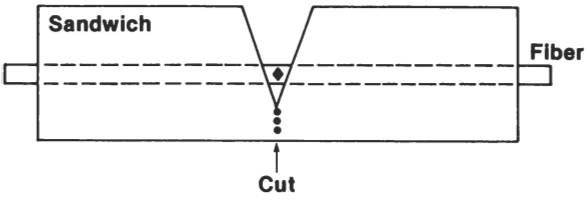

Fig. 1. Cardboard sandwich mount for protecting fiber during testing. Stripped central indentation region is exposed in V-shaped window. Mount is cut along dashed line after ends are secured in tensile loading machine.

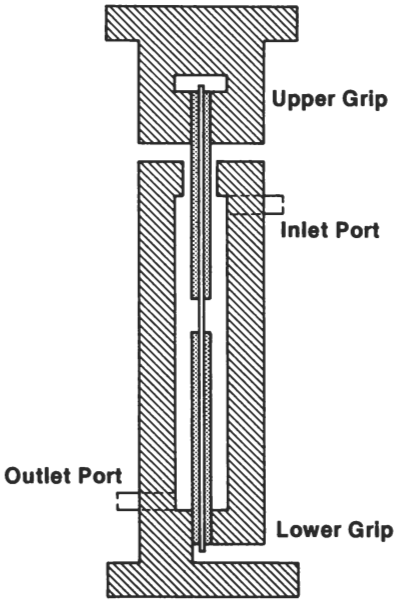

Fig. 2. Fixture for testing strength of sandwiched fiber specimens. Specimen is housed within cylindrical chamber for environmental control through ports. Section shows gripped fiber along vertical axis.

field continues to play an important role. In connection with the latter question, it is observed that radial cracks can generate spontaneously from the corners of subthreshold impressions long after completion of contact, again provided the surface is accessible to water environments.[28,29] As to the first question, Dabbs *et al.*[23] showed that crack-free indentations do indeed provide preferential failure sites in otherwise pristine borosilicate glass fibers, but that the inert strength undergoes an apparently abrupt increase on traversing the threshold into the low-load region. It would seem that the strength is governed more by the micromechanics of crack initiation than of propagation in the subthreshold domain. A subsequent dynamic fatigue study on soda-lime glass rod specimens (etched before indentation to remove spurious handling flaws)[27] showed a similar postthreshold-subthreshold discontinuity in strengths and, at the same time, a further diminution in apparent n value to about one half of the true crack velocity exponent, i.e., consistent with the factor noted earlier in connection with data from pristine surfaces. These results carry the promise of quantitative, as well as qualitative, simultations of flaw types which ultimately limit the strength properties of optical fiber components.

The present paper follows on from the earlier indentation studies by investigating the subthreshold inert and fatigue strength properties of actual fused-silica fibers. Comparative data from bulk silica glass rods are used to establish a postthreshold reference base for distinguishing between macroscopic and microscopic failure responses. An interpretation of the data in terms of current knowledge of crack initiation and propagation in glasses is offered. In this respect, it is acknowledged that fused silica has "anomalous" deformation properties, which reflect strongly in the initiation response.[32] The implications of the results concerning reliability predictions, particularly the dangers of extrapolating macroscopic crack data into the microscopic flaw region, are considered.

II. Experimental Procedure

The experimental program was conducted in two distinct parts, corresponding to subthreshold and postthreshold indentation flaw responses. For the subthreshold region, pristine optical-quality fused-silica fibers were used.* It was found to be impractical to use these same fibers for extensive characterization of the postthreshold region, however, because of premature failures during preparation (see Section II(1)) when the fibers contained radial cracks. The bulk of the data for this latter region was accordingly obtained on rod specimens of the same silica material.† Limited subthreshold tests were run on the rods to confirm the validity of data intercomparisons on either side of the threshold.

(1) Tests on Fibers: Subthreshold Flaws

Silica glass fibers 200 μm in diameter were cut into 100-mm lengths from spool-wound stock. The fiber was supplied with a protective silicone resin coating. About 10 mm of this coating was dissolved from the center region of each specimen by immersion in concentrated H_2SO_4. After the fiber was rinsed in distilled water followed by methanol and then dried in a stream of hot air, it was sandwiched between two sheets of cardboard which had been covered with slow-setting epoxy (Fig. 1). This sandwich extended over the length of the specimen but had a V-shaped window at its center so that $\approx$2 mm of the stripped region was visible. Throughout the preparation extreme caution was exercised to ensure that no physical contact was made with the exposed part of the fiber. Any specimen showing signs of contamination was discarded.

The center region of each fiber was then indented with a Vickers diamond pyramid, care being taken to clean the indenter tip of any debris between each run. Special attention was directed to alignment: the indentation load axis was brought into coincidence (to within $\pm$2 μm) of a diametral line through the fiber and the impression diagonals were oriented parallel and perpendicular to the fiber length. This procedure was to ensure a symmetrical flaw geometry relative to the subsequent tensile stress direction. All indentations were made in air at a peak contact duration of 10 s. Loads of 0.15, 0.25, and 0.50 N were used. The lowest of these loads corresponded to the limit of the hardness testing device available to us. The highest corresponded to the load above which radial cracking occasionally generated on prolonged (>1 d) postcontact aging in the laboratory atmosphere; these specimens invariably failed prematurely. In our experiments precautions were taken to keep the time between indenting and breaking to less than 1 h, and to screen each indentation microscopically immediately before the breaking test itself, to ensure that the strength data would be truly representative of the subthreshold flaw state.

Each test specimen was then secured in a crosshead testing machine with the fiber length carefully aligned along the tensile axis (Fig. 2). The end grips contacted only the outer cardboard layers, ensuring that the fiber itself was cushioned against spurious stress concentrations. At this stage the cardboard was cut at midplane, along the dotted line in Fig. 1, thereby freeing the fiber to bear the subsequently applied tensile loading. Preliminary tests on unindented specimens showed that the cardboard layers could hold the fibers without slipping up to $\approx$2 GPa longitudinal stress (computed relative to the initial cross-sectional area), a level considerably greater than that realized in the ensuing tests on indented specimens. With our arrangement, stressing rates from 0.5 to 1500 MPa$\cdot$s^{-1} were attainable. A conventional strain gage load cell was used to monitor the loading for failure times greater than a few seconds and a piezoelectric cell likewise for smaller failure times.[25] All of these tests were conducted in an environmental

*Amalgamated Wireless Ltd., Sydney, Australia.
†Herasil-F, Heraeus Quarzschelze.

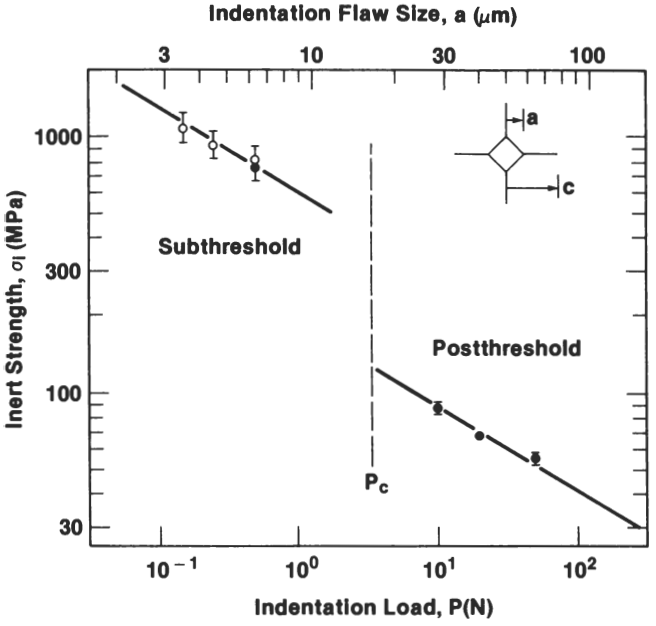

Fig. 3. Plot of inert strength of fused silica fibers (open symbols) and rods (filled symbols) as function of Vickers indentation load. Two distinct regions of behavior, corresponding to a transition from subthreshold to postthreshold flaws, are apparent. As an indicator of flaw size, hardness impression half-diagonal a is included as an alternative independent coordinate, using $H = P/2a^2 = 6.3$ GPa (Vickers hardness for silica) as the basis for converting from indentation load.

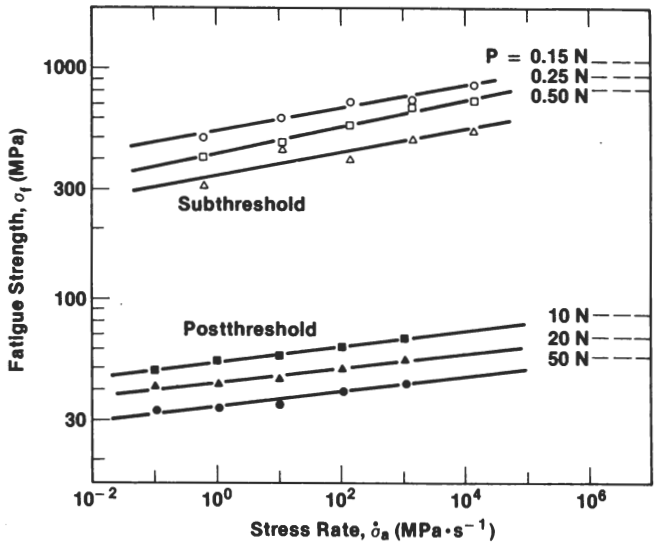

Fig. 4. Dynamic fatigue plots for fused silica fibers (open symbols) and rods (filled symbols) tested in water at Vickers indentation loads specified. Distinction between subthreshold and postthreshold regions of behavior is apparent, notably in slopes of linear fits. Standard deviation error bounds are not shown but are typically ±15% for fiber data, ±6% for rod data.

chamber (Fig. 2); dry nitrogen gas served as the environment for inert strength measurements and distilled water for dynamic fatigue measurements. After failure, the fibers were again examined microscopically to confirm that failure had originated from the indentation site. Almost invariably, the indentations split corner to corner along the median symmetry plane, producing a fracture face much the same as if radial cracks had been present all the time.

A few additional specimens were prepared for strength testing with *two* indentations in the center region at a spacing of ≈1 mm. These specimens were for examination of the *near*-critical flaw state: failure always occurred from just one of the indentations, leaving a "dummy" representative of the flaw state on the verge of instability.[25] These specimens were not included in the overall strength data pool.

(2) Tests on Rods: Postthreshold Flaws

Parallel strength data were obtained on silica rods 4 mm in diameter using a test procedure described earlier.[26,27] The rods were cut into 100-mm lengths from cane stock. These were given a pre-etch treatment in 10% HF/10% H_2SO_4 for ≈10 min to remove handling flaws from the surfaces. After the rods were rinsed and dried, they were dipped in polyurethane resin from both ends for subsequent protection, care being taken to restrict handling to the end portions until the coating was fully dried.

Vickers indentations were made in the same manner as described in Section II(1), albeit in the postthreshold region. The actual loads were 10, 20, and 50 N. Below ≈5 N the indentations did not always produce cracking, whereas above ≈100 N cracking was severe, to the extent that chipping occurred. The radial crack patterns within this load range were not always of the classical form observed in "normal" glasses;[32] spurious ring cracking was sometimes evident and the radial traces tended to emerge from points on the impression perimeter away from the corners. Those specimens without well-defined radial cracks perpendicular to the rod axis were eliminated.

The acceptable specimens were broken, within 1 h of indentation, in four-point flexure. The flexure apparatus was constructed in accordance with ASTM specifications,[33] inner span 20 mm and outer span 60 mm. Special care was again taken to orient the indentations at the maximum tensile surface.[26] The equipment for delivering and monitoring the breaking load was the same as described in Section II(1). For the rods, the range of available stressing rates was 0.1 to 1000 MPa·s^{-1}. A dry environment for inert strength measurements was obtained by encasing the test specimen in a plastic sleeve through which nitrogen gas could be blown. Dynamic fatigue measurements were made with the indentation site covered by a drop of distilled water. All failures in the postthreshold load range were found to originate from the radial cracks.

Some additional specimens were prepared, as with the fibers, with dummy indentations for characterization of the critical flaw state.[25,26] Another set of controls was prepared with 0.50 N indentations for comparison with the corresponding fiber data.

III. Results

The results of the strength tests on the fused silica fiber and rod specimens are summarized in Figs. 3 and 4. Each data point represents the mean and standard deviation (computed in logarithmic coordinates) of at least 10 fiber specimens or 4 rod specimens (although the error bars are not shown explicitly in Fig. 4, to avoid data overlap). The lines through these points are analytical fits, as described next.

(1) Inert Strengths

Figure 3 is a plot of the inert strength, σ_i, as a function of the indentation load, P. These data were obtained at the fastest stressing rate available with our apparatus to minimize a possible fatigue effect from trace moisture in the nitrogen environment. It is immediately clear that there are two distinct regions of behavior, according to whether the load is greater or less than the threshold value, P_c. In particular, note the apparent discontinuity in the strength function $\sigma_i(P)$; the subthreshold strengths are significantly higher than the values that we would predict by extrapolation from the postthreshold data. The overlap at $P = 0.50$ N between data points for rods and fibers confirms that this discontinuity is no mere artifact resulting from changes in specimen configuration. As mentioned in Section I, such behavior is consistent with a transition from propagation-controlled to initiation-controlled failure. The increased scatter in the subthreshold data region is worth noting in this context.

The dummy indentation experiments referred to in Section II provided more direct information on the issue of propagation- vs initiation-controlled failure. For the rod specimens with post-

Table I. Parameters for Fused Silica from Strength Data

	Postthreshold	Subthreshold	Units
Inert	$\eta' = 190 \pm 12$	$\eta'' = 603 \pm 70$	$MPa \cdot N^{1/3}$
Fatigue*	$n' = 30.7 \pm 0.8$	$n'' = 19.0 \pm 1.5$	
	$\log \lambda_P' = 62.7 \pm 0.5$	$\log \lambda_P'' = 50.6 \pm 2.7$	†

*Water environment. †Evaluated for σ_f in MPa, $\dot{\sigma}_a$ in $MPa \cdot s^{-1}$.

threshold flaws, the surviving dummy indentations indicated a significant radial crack extension (≈50%) in the direction perpendicular to the tensile axis.‡ This precursor growth enroute to failure reflects the stabilizing influence on the equilibrium failure configuration exerted by the residual-contact driving forces.[19–26] By contrast, for the fiber specimens the dummy indentations showed no signs of any radial cracking at all at the low loads used. Failure in this case appears to have generated spontaneously from within the hardness impression. Thus from a fracture mechanics standpoint, it is only in the postthreshold region that we are able to define a well-developed crack system for determining the critical failure condition.

It is therefore not surprising that detailed theoretical formulations of the function $\sigma_i(P)$ for comparison with such data as in Fig. 3 are currently available only for postthreshold indentation flaws. The essence of this formulation is surveyed in Ref. 34. One begins by writing down a stress intensity function for pennylike radial cracks subjected both to residual-contact and external driving forces, $K = K(c, P, \sigma_a)$, where c is the crack size, P the indentation load, and σ_a the applied stress.[18,19] Then the requirement for unstable equilibrium, $dK/dc \geq 0$ at $K = K_c$, where K_c defines the "toughness," is invoked. This gives the result[26,34]

$$\sigma_i = \eta'/P^{1/3} \tag{1}$$

where $\eta' = \eta'(K_c)$ is a material constant.§ (Here single- and double-prime notation will be used to distinguish postthreshold and subthreshold parameters.) The solid line through the postthreshold data points in Fig. 3 is a best fit in accordance with Eq. (1). In the absence of an analogous relation for subthreshold flaws we have tentatively applied the same fitting procedure to the fiber data. The values of the parameters η' and η'' obtained from these fits are given in Table I. The relative values of these parameters usefully quantify the difference in mechanical response in the two flaw states.

(2) *Fatigue Strengths*

Plots of the dynamic fatigue strength, σ_f, as a function of applied stressing rate, $\dot{\sigma}_a$, are given in Fig. 4 for each specified indentation load, P. The horizontal broken lines at right in these plots indicate the corresponding upper-bound inert strength levels from Fig. 3. It is again apparent, from the slopes as well as from the strength levels and the scatter, that the mechanical response is different above and below the threshold load.

As in the previous subsection, a detailed fracture mechanics description for analyzing the data in Fig. 4 has been developed only for the postthreshold configuration.[34] To obtain a dynamic fatigue relation, the same stress intensity function as before (Section III(1)) is used to define the net crack driving force. This time, however, a crack velocity equation, $v = v_0(K/K_c)^n$, governs the crack extension, where n and v_0 are material-environment parameters. The solution of the differential equation which results from the combination of these expressions is of the familiar form[21,24,26,34,35]

$$\sigma_f = (\lambda' \dot{\sigma}_a)^{1/(n'+1)} \tag{2}$$

The parameter n' is of special interest, for it determines the "susceptibility" (strictly, the inverse susceptibility) to fatigue effects, as mentioned in Section I. For idealized flaws free of all residual-stress influences, n' identifies with the crack velocity exponent n.[21] For the more general case of interest here where residual driving forces are by no means negligible, the parametric connection is less direct. The analysis gives[34,35]

$$n' = 3n/4 + 1/2 \tag{3a}$$

$$\lambda' = \lambda_P'/P^{(n'-2)/3} \tag{3b}$$

where $\lambda_P' = \lambda_P'(n, v_0, K_c)$ is a load-independent constant for the material-environment system. According to Eqs. (2) and (3), the function $\sigma_f(\dot{\sigma}_a)$ at different P should plot as a family of parallel straight lines on a dynamic fatigue diagram, at least in the postthreshold region.

The solid lines in Fig. 4 are appropriate best fits to each data set. In extending this linear fitting scheme to loads at $P < P_c$ we acknowledge, as with the inert strength analysis, that no physical significance should be attached to the subthreshold parameters n'' and λ'' evaluated from Eq. (2). Certainly we cannot expect the connecting relations in Eq. (3) to remain valid in this region, for these relations are based on far-field approximations in the residual-contact $K(c, P)$ function.[18,20] With this qualification, we plot the slope and intercept parameters from Fig. 4 as a function of indentation load in Fig. 5. For the rod data, at $P > P_c$, the n' parameter plots independently of P, as required by Eq. (3*a*). The solid line is an averaged representation over the individual mean values in this load range. On the other hand, the corresponding λ' parameter depends on P. In this case the solid line is a representation of Eq. (3*b*) at constant λ_P', fitted in accordance with the averaged n' value from the upper plot. Similar fits to the fiber data at $P < P_c$ are indicated in Fig. 5. The results of the parametric evaluations from these fits are included in Table I. Once again, the relative values of the parameters for the two flaw states serve to highlight the difference in mechanical response.

IV. Discussion

The results in the previous section indicate distinct changes in strength properties on traversing the postthreshold-subthreshold indentation flaw transition load. These changes are seen most clearly in the graphical constructions of Figs. 3 and 5 and in the parametric evaluations of Table I. We may summarize the three major features as follows:

(1) An increase in the inert strength, by a factor $\eta''/\eta' \approx 3$. The subthreshold indentations do not have well-developed radial cracks, yet remain preferred sites for fracture. Tests on fibers with dummy indentations show corner-to-corner failure from the critical flaw, but no crack pop-in at the surviving flaw. This behavior indicates that the subthreshold flaws do ultimately fail by the same, unlimited radial fracture mode as their postthreshold counterparts, but that this fracture mode has to overcome an initiation behavior.

(2) An increase in the fatigue susceptibility, as reflected inversely by the ratio $n''/n' \approx \frac{2}{3}$. From macroscopic crack tests on fused silica in water, values for the true crack velocity exponent in the range $n = 36$ to 41 are reported.[16,17] These values may be compared with the estimate $n = 40.3 \pm 1.1$ from the present dynamic fatigue data for postthreshold flaws, obtained by inserting n' into Eq. (3*a*). The level of self-consistency here allows us to assert that the radial flaws behave in the same way as large-scale cracks right down to the threshold load. The apparent reduction in velocity

‡Quantitatively, using the scheme outlined in Ref. 26 for reducing crack-size data at different loads, we find $c_0'/P^{2/3} = 9.7 \pm 1.4\ \mu m/N^{2/3}$ immediately before strength testing (254 cracks) and $c_m/P^{2/3} = 15.2 \pm 2.7\ \mu m/N^{2/3}$ at the critical configuration (21 cracks).

§Strictly, η' also depends on the hardness-to-modulus ratio H/E, but this dependence is weak and is of no relevance here (Ref. 20).

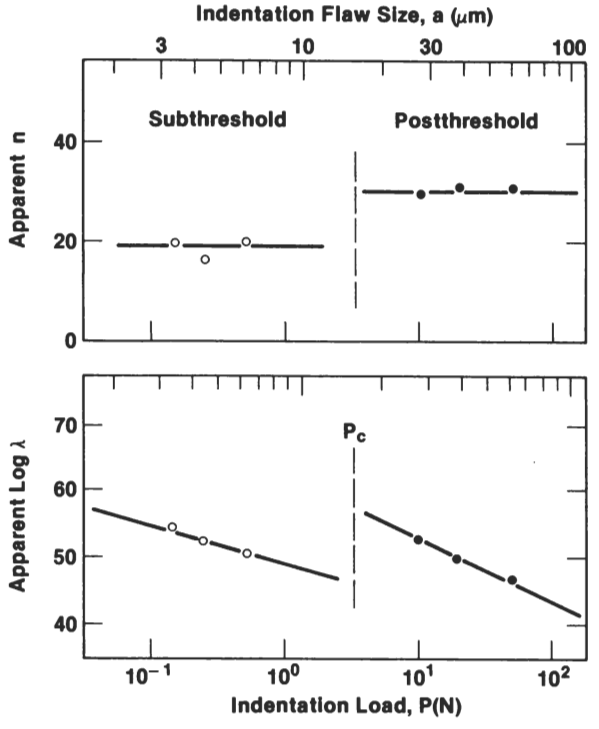

Fig. 5. Plots of apparent n and λ parameters from data fits of Fig. 4 as a function of appropriate indentation loads. (λ has units as evaluated in Table I.) Indentation flaw size axis at top is plotted as in Fig. 3.

exponent for the indentation flaws in this region, $n'/n \approx 3/4$, is a measure of the residual-stress influence in the dynamic fatigue response. On entering the domain of subthreshold indentations this ratio reduces further, to $n''/n \approx 1/2$, suggesting that the residual influence is even stronger in the initiation micromechanics.

(3) An increase in scatter in data, as reflected by the relatively large error bounds at $P < P_c$ in Figs. 3 and 4. This trend is consistent with a change in fracture mechanics where the characteristics of the near field rather than of the far field of the residual indentation control the flaw response. Near contact fields are far more inhomogeneous in their spatial distribution[36] and are correspondingly more sensitive to local fluctuations in the deformation processes which constitute the hardness zone.

Hence as we approach the domain of ultrahigh strengths, our focus shifts to the more complex issue of crack initiation. In an earlier attempt to model this phase of the fracture process a phenomenological approach was adopted, assuming that the crack nucleus can be regarded as an incipient microcrack in a local field determined by the scale of the hardness zone.[31] This model, in circumventing any reference to the explicit deformation processes which generate the crack nucleus in the first place, may be seen to be somewhat restrictive in the present context. The question as to how the residual component of the contact field enters the picture is obscure; and we have emphasized the crucial role of the residual driving force for fracture in all stages of flaw evolution. Again, we have mentioned that fused silica is an "anomalous" glass insofar as its deformation properties are concerned;[32] is it valid to apply a model derived on the implicit assumption of "normal" behavior to such glasses? In the absence of a theoretical base for incorporating these and other essential physical elements of the initiation process, we have no proper foundation for using fracture mechanics as a predictive tool in strong-fiber applications at all.

Nevertheless, some more recent experimental observations of the near-contact deformation zone in glasses appear to be providing us with the necessary physical understanding for setting up a sounder model.[28–30,37,38] At present, developments along these lines have not gone beyond the qualitative stage. Essentially, the evolution of radial cracks in a sharp-indenter field is envisaged as

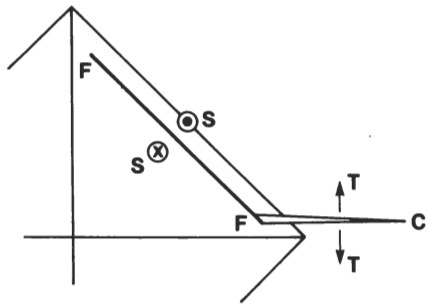

Fig. 6. Two-step process for crack initiation in indented glass. Stress concentration develops at edge of constrained fault FF in quadrant of Vickers impression, thereby generating microcrack FC. Shear (S) and tensile (T) stress components responsible for driving respective steps are indicated (after Ref. 28).

a two-step process.[28,29] This process is depicted schematically in Fig. 6. In the first, precursor step the penetrating indenter generates shear displacements into the material from the contact surface. These displacements occur on well-defined "fault" surfaces, at discrete spatial intervals, typically at ≈ 1 μm separation, at shear stresses close to the theoretical limit of the glass. The faulting accounts for only part of the deformation, however, since the open glass network is also amenable to structural densification.[39,40] It is here that the major distinction arises between normal and anomalous glasses. In the latter there is less ionic modifier content in the structure to provide "easy slip" paths for cooperative shear processes,[39] in which case the faults tend to be confined to the near-surface region.[29] Consequently, densification is the dominant deformation mode in anomalous glasses; and since this mode is better able to accommodate the indentation volume than is the competitive shearing mode, the residual contact field is much less intense than in normal glasses.[32]

In the second step of the initiation process a microcrack generates at the edge of a critical fault, where the locked-in shear stresses are concentrated.[28] It is believed that generation takes place close to the specimen free surface, thus accounting for the sensitivity of subthreshold phenomena to environmental interactions as alluded to in Section III. It is also believed that this phase of the flaw development is common to normal and anomalous glass types, notwithstanding the distinctive deformation responses described.[29] It is only the geometrical constraints that differ in the two glass types. This would explain why the same three major features in strength properties for fused silica listed at the start of this section are observed also in soda-lime glass (the archetypal normal glass).[27]

Let us now reexamine these three features in terms of the two-step process just outlined. We expect the inert strength in the subthreshold region to exceed that predicted on the basis of extrapolation from postthreshold data because, put simply, the microcrack configuration in Fig. 6 is not nearly as potent a flaw as the well-developed radial crack. The fact that radial cracking can generate spontaneously in the postindentation configuration (at loads just below P_c, in moist environments)[28] means that the local residual driving force must overcome some initiation barrier. Subsequently applied tensile stresses will augment these driving forces, thereby lowering the barrier. The indication in our observation of subthreshold dummy flaws at loads $P \ll P_c$ is that the barrier persists at stress levels which would cause equivalent postthreshold flaws to become unstable, i.e., as defined by Eq. (1). Hence the increase in strength evident in Fig. 3. Clearly, the key to a quantitative description of this strength trend is an analytical expression for the subthreshold driving force, analogous to the stress intensity function $K(c, P, \sigma_a)$ from which Eq. (1) derives (Section III(1)), embodying the characteristic elements of both the faulting and the microcracking stages indicated in Fig. 6.

As to the increase in fatigue susceptibility observed in the low-

load region, theoretical fracture mechanics tells us that the more dominant is the residual-stress contribution to the net driving force, the stronger is the depression of the indentation fatigue parameter n' below the true velocity exponent n. (For instance, in going from point-contact to line-contact flaws the "range" of the residual field increases, with consequent reduction of n'/n in Eq. (3*a*) from $\approx 3/4$ to $\approx 1/2$.[35]) Following our conclusions in the previous paragraph concerning the initiation barrier, we would certainly expect the residual stresses to exert a greater influence on the mechanical response while the crack remains in the near vicinity of the shear fault. This would account for a ratio n''/n' less than unity. Again, the derivation of an appropriate analogue to the postthreshold relation Eq. (3*a*) allowing for an exact determination of this ratio (contingent, of course, on the retention of Eq. (2) as a valid descriptor in the subthreshold region) awaits a more detailed analytical model.

This leaves the issue of the increased scatter. We have already mentioned the sensitivity of fracture phenomena in the near-contact-region to stress-field inhomogeneity. Microscopic examinations of the fault patterns show a marked lack of geometrical reproducibility from indentation to indentation; indeed, the surface traces do not even show a symmetrical disposition in the four quadrants of the hardness impression for any given indentation.[28] Bearing in mind that we are talking about faults spaced at ≈ 1 μm in flaws of size $\lesssim 5$ μm (Figs. 3 and 5), it becomes clear that there is scope for a strong stochastical element in the initiation micromechanics.

We have described experimental results from specimens containing artificially introduced flaws. Are we justified in using these results to infer the mechanical response of optical fibers containing "natural" flaws? From a fracture mechanics standpoint it can be demonstrated that the existence of a size-dependent threshold is a general phenomenon, especially in association with flaws initially generated in highly concentrated stress fields (contact sites, particle inclusions, etc.).[35,41,42] Thus abrupt changes in measured strength parameters, corresponding to a transition from propagation-controlled to indentation-controlled fracture processes, should not be an altogether unexpected occurrence in systems where special efforts are made to refine the flaw distributions toward the ultimate in surface perfection. Reference was made earlier (Section I) to a fatigue susceptibility parameter ≈ 20 reported by several workers for pristine silica fibers tested in water. This value does not appear to be too sensitive to "light" surface damage[10,11] (such that the strengths remain in the region $\gtrsim 1$ GPa), but fibers degraded by a relatively severe abrasion treatment show a substantial increase, to between 29 to 37.[43,44] These values may be compared with the respective parameters $n' = 19.0$ and $n' = 30.7$ for the subthreshold and postthreshold indentation flaws in the present study. Although it might be unwise to attach unequivocal significance to the quantitative correspondence here, the results do at least give confidence in using controlled flaws to predict trends in fiber strength properties.

This last point is one that should appeal to those who seek a deeper understanding of the fundamental physical and chemical processes which determine the mode of failure in the ultra-high-strength region. First, the facility to create one's own flaws in a controlled manner allows for detailed study of underlying structural micromechanisms at all stages of the evolution, from first inception to ultimate failure. This is an aspect of fracture mechanics which has been largely ignored by the glass testing community, particularly in relation to optical fibers. We have intimated in this section that studies of this kind can lead to unexpected conclusions; the crucial role of residual crack driving forces in parametric evaluations is a case in point. Second, indentation testing ensures optimal reproducibility in strength data, thus lending itself to a more systematic investigation of material-environment variables (glass composition, environmental chemistry, temperature, etc.) than currently available with statistical-based methodologies. By fixing the flaw configurations one establishes a sounder basis for comparative evaluation of extraneous influences on fiber strength properties, e.g., in using data from coated and uncoated fibers to determine the role of protective layers in fatigue processes.

Finally, there are some implications concerning design and reliability which warrant brief comment. Most current design procedures derive from the unqualified acceptance of the simplistic "Griffith flaw" concept. That is, it is assumed that the flaws are exclusively cracklike in nature and are totally free of preexisting influences. We have presented evidence which questions both of these assumptions, particularly in the ultrasmall flaw region so pertinent to optical fibers. This is not to say that the conventional strength formalisms may not provide reasonable empirical fits to laboratory test data. After all, Eq. (2) has exactly the same form as the familiar dynamic fatigue equation for Griffith cracks, yet it provides linear fits to our data for postthreshold and subthreshold flaws in Fig. 4. It is in the parameters obtained from such fits that the main differences reside. In particular, one has to be extremely cautious in attempting to predict these parameters for any flaw type from macroscopic crack velocity data. For this kind of prediction it is necessary to employ the appropriate parametric connecting relations (analogous to our Eq. (3) for residually stressed post-indentation flaws). But perhaps most important of all is the potential danger in data extrapolations beyond the laboratory testing range, notably to long operational lifetimes. The observation that flaws can continue to evolve long after inception if conditions are "right" (undiminished residual stress, reactive environment, elevated temperature)[28,29] is a cause for concern in this regard. Thus we might take every possible precaution to guarantee an "acceptably high" strength level for our finished fiber product (e.g., by fatigue testing unlimited numbers of control specimens, proof testing), but all of this will count for nothing if the controlling flaw undergoes a subthreshold-postthreshold transition at some later stage during service. There is in fact some evidence in the glass fiber literature to suggest that lifetime characteristics can suffer abrupt changes on prolonged exposure to water.[2] This phenomenon is surely one area of research that bears further investigation.

References

[1] J. T. Krause, C. R. Kurkjian, and U. C. Paek, "Tensile Strengths >4 GPa for Lightguide Fusion Splices," *Electron. Lett.*, **17** [21] 812–13 (1981).

[2] H. C. Chandan and D. Kalish, "Temperature Dependence of Static Fatigue of Optical Fibers Coated with a UV-Curable Polyurethane Acrylate," *J. Am. Ceram. Soc.*, **65** [3] 171–73 (1982).

[3] C. R. Kurkjian and U. C. Paek, "Single-Valued Strength of 'Perfect' Silica Fibers," *Appl. Phys. Lett.*, **42** [3] 251–53 (1983).

[4] D. Kalish, B. K. Tariyal, and R. O. Pickwick, "Static and Dynamic Fatigue of Fused Silica Optical Fibers"; for abstract see *Am. Ceram. Soc. Bull.*, **56** [3] 332 (1977).

[5] L. A. Jackson and M. H. Reeve, "A Technique for Estimating the Breaking Strain of Long Lengths of Optical Fibers," *J. Phys. E: Sci. Instrum.*, **11** [2] 161–65 (1978).

[6] D. Kalish and B. K. Tariyal, "Static and Dynamic Fatigue of a Polymer-Coated Fused Silica Optical Fiber," *J. Am. Ceram. Soc.*, **61** [11–12] 518–23 (1978).

[7] J. E. Ritter, J. M. Sullivan, and K. Jakus, "Application of Fracture Mechanics Theory to Fatigue Failure of Optical Glass Fibers," *J. Appl. Phys.*, **49** [9] 4779–82 (1978).

[8] H. Schonhorn, T. T. Wang, H. N. Vazirani, and H. L. Frisch, "Static and Dynamic Fatigue of High-Strength Glass Fibers Coated with a UV Curable Epoxy Acrylate," *J. Appl. Phys.*, **49** [9] 4783–87 (1978).

[9] Y. Mitsunaga, Y. Katsuyama, H. Kobayashi, and Y. Ishida, "Failure Predictions for Long Length Optical Fiber Based on Proof Testing," *J. Appl. Phys.*, **53** [7] 4847–53 (1982).

[10] S. P. Craig, W. J. Duncan, P. W. France, and J. E. Snodgras, "The Strength and Fatigue of Large Flaws in Silica Optical Fiber": Paper AVI-4, presented at the 8th ECOC Conference, Cannes, 1982.

[11] F. A. Donaghy and D. R. Nicol, "Evaluation of the Fatigue Constant n in Optical Fibers with Surface Particle Damage," *J. Am. Ceram. Soc.*, **66** [8] 601–604 (1983).

[12] S. M. Wiederhorn; pp. 613–46 in Fracture Mechanics of Ceramics, Vol. 2. Edited by R. C. Bradt, D. P. H. Hasselman, and F. F. Lange. Plenum Press, New York, 1974.

[13] A. G. Evans and H. Johnson, "The Fracture Stress and Its Dependence on Slow Crack Growth," *J. Mater. Sci.*, **10** [2] 214–22 (1975).

[14] J. E. Ritter; pp. 667–86 in Fracture Mechanics of Ceramics, Vol. 4. Edited by R. C. Bradt, D. P. H. Hasselman, and F. F. Lange. Plenum Press, New York, 1978.

[15] J. E. Ritter; to be published in Strength of Glass. Edited by C. R. Kurkjian. Plenum Press, New York.

[16] S. M. Wiederhorn; quoted on p. 58 of Glass: Science and Technology, Vol. 5. Edited by D. R. Uhlmann and N. J. Kreidl. Academic Press, New York, 1980.

[17] S. Sakaguchi, Y. Sawaki, Y. Abe, and T. Kawasaki, "Delayed Failure in Silica Glass," *J. Mater. Sci.*, **17** [10] 2878–86 (1982).

[18] D. B. Marshall and B. R. Lawn, "Residual Stress Effects in Sharp-Contact Cracking: I," *J. Mater. Sci.*, **14** [9] 2001–12 (1979).

[19] D. B. Marshall, B. R. Lawn, and P. Chantikul, "Residual Stress Effects in Sharp-Contact Cracking: II," *J. Mater. Sci.*, **14** [9] 2225–35 (1979).

[20] B. R. Lawn, A. G. Evans, and D. B. Marshall, "Elastic/Plastic Indentation Dam-

age in Ceramics: The Median/Radial Crack System," *J. Am. Ceram. Soc.*, **63** [9–10] 574–81 (1980).
[21]D. B. Marshall and B. R. Lawn, "Flaw Characteristics in Dynamic Fatigue: The Influence of Residual Contact Stresses," *J. Am. Ceram. Soc.*, **63** [9–10] 532–36 (1980).
[22]P. Chantikul, B. R. Lawn, and D. B. Marshall, "Micromechanics of Flaw Growth in Static Fatigue: Influence of Residual Contact Stresses," *J. Am. Ceram. Soc.*, **64** [6] 322–25 (1981).
[23]T. P. Dabbs, D. B. Marshall, and B. R. Lawn, "Flaw Generation by Indentation in Glass Fibers," *J. Am. Ceram. Soc.*, **63** [3–4] 224–25 (1980).
[24]B. R. Lawn, D. B. Marshall, G. R. Anstis, and T. P. Dabbs, "Fatigue Analysis of Brittle Materials Using Indentation Flaws: I," *J. Mater. Sci.*, **16** [10] 2846–54 (1981).
[25]R. F. Cook, B. R. Lawn, and G. R. Anstis, "Fatigue Analysis of Brittle Materials Using Indentation Flaws: II," *J. Mater. Sci.*, **17** [4] 1108–16 (1982).
[26]T. P. Dabbs, B. R. Lawn, and P. L. Kelly, "A Dynamic Fatigue Study of Soda-Lime Silicate and Borosilicate Glasses Using Small-Scale Indentation Flaws," *Phys. Chem. Glasses*, **23** [2] 58–66 (1982).
[27]T. P. Dabbs and B. R. Lawn, "Fatigue of High-Strength Soda-Lime Glass: A Constant Stressing Rate Using Subthreshold Indentation Flaws," *Phys. Chem. Glasses*, **23** [4] 93–97 (1982).
[28]B. R. Lawn, T. P. Dabbs, and C. J. Fairbanks, "Kinetics of Shear-Activated Indentation Crack Initiation in Soda-Lime Glass," *J. Mater. Sci.*, **18** [9] 2785–97 (1983).
[29]H. Multhopp, B. R. Lawn, and T. P. Dabbs; pp. 681–93 in Deformation of Ceramic Materials II. Edited by R. E. Tressler and R. C. Bradt. Plenum Press, New York, 1984.
[30]T. P. Dabbs, C. J. Fairbanks, and B. R. Lawn; pp. 142–53 in Structural Reliability of Brittle Materials. Edited by S. W. Freiman and C. M. Hudson. *ASTM Spec. Tech. Publ.*, **No. 844** (1984).
[31]B. R. Lawn and A. G. Evans, "A Model for Crack Initiation in Elastic/Plastic Indentation Fields," *J. Mater. Sci.*, **12** [11] 2195–99 (1977).
[32]A. Arora, D. B. Marshall, B. R. Lawn, and M. V. Swain, "Indentation Deformation/Fracture of Normal and Anomalous Glasses," *J. Non-Cryst. Solids*, **31** [3] 415–28 (1979).
[33]ASTM Designation C158; p. 111 in 1976 Annual Book of ASTM Standards, Part 17. American Society for Testing and Materials, Philadelphia, PA.
[34]R. F. Cook and B. R. Lawn; pp. 22–42 in Structural Reliability of Brittle Materials. Edited by S. W. Freiman and C. M. Hudson. *ASTM Spec. Tech. Publ.*, **No. 844** (1984).
[35]E. R. Fuller, B. R. Lawn, and R. F. Cook, "Theory of Fatigue for Brittle Flaws Originating from Stress Concentrations," *J. Am. Ceram. Soc.*, **66** [5] 314–21 (1983).
[36]B. R. Lawn and T. R. Wilshaw, "Indentation Fracture: Principles and Applications," *J. Mater. Sci.*, **10** [6] 1049–81 (1975).
[37]J. T. Hagan, "Cone Cracks Around Vickers Indentation in Fused Silica," *J. Mater. Sci.*, **14** [2] 462–66 (1979).
[38]J. T. Hagan, "Shear Deformation Under Pyramidal Indentations in Soda-Lime Glass," *J. Mater. Sci.*, **15** [6] 1417–24 (1980).
[39]F. M. Ernsberger, "Mechanical Properties of Glass," *J. Non-Cryst. Solids*, **22** [1–3] 293–321 (1977).
[40]I. Yasui and M. Imaoka, "Finite Element Analysis of Indentation on Glass (II)," *J. Non-Cryst. Solids*, **50** [2] 219–32 (1982).
[41]K. E. Puttick, "Energy Scaling, Size Effects and Ductile-Brittle Transitions in Fracture," *J. Phys. D: Appl. Phys.*, **12** [3] L19–L23 (1979).
[42]D. J. Green; pp. 457–78 in Fracture Mechanics of Ceramics, Vol. 5. Edited by R. C. Bradt, A. G. Evans, D. P. H. Hasselman, and F. F. Lange. Plenum Press, New York, 1983.
[43]W. E. Snowden and Ben Justice, "Effect of Cladding Composition on Stress Corrosion and Fatigue of Optical Waveguide Fibers," *J. Am. Ceram. Soc.*, **59** [9–10] 452–53 (1976).
[44]S. T. Gulati, J. D. Helfinstine, B. Justice, J. S. McCartney, and M. A. Runyan, "Measurement of Stress Corrosion Constant *n* for Optical Fibers," *Am. Ceram. Soc. Bull.*, **58** [11] 1115–17 (1979).